The effect of core asymmetries on the polarization properties of hollow core photonic bandgap fibers

F. Poletti, N. G. R. Broderick, and D. J. Richardson
Optoelectronic Research Centre, University of Southampton, SO17 1BJ, UK
frap@orc.soton.ac.uk

T. M. Monro
School of Chemistry & Physics, University of Adelaide, Adelaide SA 5005, Australia

Abstract: We present the results of numerical simulations of the modal properties of Photonic Band Gap Fibers (PBGFs) in which a structural distortion of the silica ring surrounding the air core is gradually introduced. We demonstrate that surface modes supported within such fibers are very sensitive to structural distortions, and that any asymmetric change in the structure can break their degeneracy resulting in associated changes in the anticrossing behavior of the orthogonally polarized core modes, and the development of polarization dependent transmission properties. Our results provide insight into recent experimental observations of wavelength dependent PDL and birefringence in PBGFs.

OCIS codes: : (060.2280) Fiber design and fabrication; (060.2400) Fiber properties; (260.1440) Birefringence

References and links

1. R. F. Cregan, B. J. Mangan, J. C. Knight, T. A. Birks, P. S. Russell, P. J. Roberts, and D. C. Allan, "Single-mode photonic band gap guidance of light in air," Science **285**, 1537–1539, (1999).
2. D. G. Ouzounov, F. R. Ahmad, D. Muller, N. Venkataraman, M. T. Gallagher, M. G. Thomas, J. Silcox, K. W. Koch, and A. L. Gaeta, "Generation of megawatt optical solitons in hollow-core photonic band-gap fibers," Science **301**,1702–1704, (2003).
3. P. J. Roberts, F. Couny, H. Sabert, B. J. Mangan, D. P. Williams, L. Farr, M. W. Mason, A. Tomlinson, T. A. Birks, J. C. Knight, and P. S. J. Russell, "Ultimate low loss of hollow-core photonic crystal fibres," Opt. Express **13**, 236–244, (2005), http://www.opticsexpress.org/abstract.cfm?URI=OPEX-13-1-236
4. T. J. Stephens, R. R. Maier, J. S. Barton and J. D. C. Jones, "Fused silica hollow-core photonic crystal fibre for mid-infrared transmission," presented at Conference on Lasers and Electro-Optics (CLEO); Postconference Digest, CPDD4, 16-21 May 2004, San Francisco, CA, USA, (2004).
5. K. Saitoh and M. Koshiba, "Photonic bandgap fibers with high birefringence," IEEE Photonics Technol. Lett. **14**, 1291–1293, (2002).
6. X. Chen, M.-J. Li, N. Venkataraman, M. T. Gallagher, W. A. Wood, A. M. Crowley, J. P. Carberry, L. A. Zenteno, and K. W. Koch, "Highly birefringent hollow-core photonic bandgap fiber," Opt. Express **12**, 3888–3893 (2004), http://www.opticsexpress.org/abstract.cfm?URI=OPEX-12-16-3888
7. M. S. Alam, K. Saitoh, and M. Koshiba, "High group birefringence in air-core photonic bandgap fibers," Opt. Lett. **30**, 824–826, (2005).
8. M. T. Steel, T. P. White, C. M. De Sterke, R. C. McPhedran, and L. C. Botten, "Symmetry and degeneracy in microstructured optical fibers," Opt. Lett. **26**, 488–90 (2001).
9. G. Bouwmans, F. Luan, J. C. Knight, P. S. J. Russell, L. Farr, B. J. Mangan, and H. Sabert, "Properties of a hollow-core photonic bandgap fiber at 850 nm wavelength," Opt. Express **11**, 1613–1620 (2003), http://www.opticsexpress.org/abstract.cfm?URI=OPEX-11-14-1613

#8732 - $15.00 USD Received 8 September 2005; revised 25 October 2005; accepted 25 October 2005

10. T. D. Engeness, M. Ibanescu, S. G. Johnson, O. Weisberg, M. Skorobogatiy, S. Jacobs, and Y. Fink, "Dispersion tailoring and compensation by modal interactions in omniguide fibers," Opt. Express **11**, 1175–1196, (2003), http://www.opticsexpress.org/abstract.cfm?URI=OPEX-11-10-1175
11. G. Humbert, J. C. Knight, G. Bouwmans, P. S. Russell, D. P. Williams, P. J. Roberts, and B. J. Mangan, "Hollow core photonic crystal fibers for beam delivery," Opt. Express **12**, 1477–1484, (2004), http://www.opticsexpress.org/abstract.cfm?URI=OPEX-12-8-1477
12. M. Wegmuller, M. Legre, N. Gisin, T. P. Hansen, C. Jacobsen, and J. Broeng, "Experimental investigation of the polarization properties of a hollow core photonic bandgap fiber for 1550 nm," Opt. Express **13**, 1457–1467 (2005), http://www.opticsexpress.org/abstract.cfm?URI=OPEX-13-5-1457
13. N. A. Mortensen and M. D. Nielsen, "Modeling of realistic cladding structures for air-core photonic bandgap fibers," Opt. Lett. **29**, 349–351 (2004).
14. K. Saitoh, N. A. Mortensen, and M. Koshiba, "Air-core photonic band-gap fibers: the impact of surface modes," Opt. Express **12**, 394–400 (2004), http://www.opticsexpress.org/abstract.cfm?URI=OPEX-12-3-394
15. C. M. Smith, N. Venkataraman, M. T. Gallagher, D. Muller, J. A. West, N. F. Borrelli, D. C. Allan, and K. W. Koch, "Low-loss hollow-core silica/air photonic bandgap fibre," Nature **424**, 657–659, (2003).
16. F. Poletti, V. Finazzi, T. M. Monro, N. G. R. Broderick, V. Tse, and D. J. Richardson, "Inverse design and fabrication tolerances of ultra-flattened dispersion holey fibers," Opt. Express **13**, 3728–3736, (2005), http://www.opticsexpress.org/abstract.cfm?URI=OPEX-13-10-3728
17. P. R. McIsaac, "Symmetry-induced modal characteristics of uniform waveguides. i. summary of results," IEEE Trans. Microwave Theory Tech. **23**, 421–429, (1975).
18. M. Koshiba and K. Saitoh, "Finite-element analysis of birefringence and dispersion properties in actual and idealized holey-fiber structures," Appl. Opt. **42**, 6267–6275, (2003).
19. D. C. Allan, N. F. Borrelli, M. T. Gallagher, D. Muller, C. M. Smith, N. Venkataraman, J. A. West, P. Zhang, and K. W. Koch, "Surface modes and loss in air-core photonic band-gap fibers," in *Photonic Crystal Materials and Devices*, Proc. SPIE **5000**, 161–174, (2003).
20. J. A. West, C. M. Smith, N. F. Borrelli, D. C. Allan, and K. W. Koch, "Surface modes in air-core photonic band-gap fibers," Opt. Express **12**, 1485–1496 (2004), http://www.opticsexpress.org/abstract.cfm?URI=OPEX-12-8-1485

1. Introduction

The possibility of realizing microstructured optical fibers in which light is confined to the core by means of photonic bandgap effects has attracted significant interest in recent years since it enables light guidance in a low refractive index material such as air, vacuum or gas [1]. Photonic Bandgap fibers (PBGF) in which a high percentage of the light can be guided in a hollow core offer amongst other opportunities the possibility of significantly reducing the nonlinearities with respect to silica core fibers [2], the potential to achieve lower losses than conventional doped solid core fibers [3], as well as the possibility of transmitting light at wavelengths where the material absorption would otherwise be prohibitive [4].

In order to design PBGFs for device and system applications it is essential to establish a detailed understanding of the polarization properties of such fibers [e.g. birefringence, polarization-dependent loss (PDL) and polarization mode dispersion (PMD)], to determine how these properties depend on the fiber structure, and to establish means of controlling these during fabrication, and/or use. One way to limit the interactions between the two nearly degenerate orthogonal fundamental modes (FMs) is to deliberately fabricate highly birefringent, polarization-maintaining structures. PBGFs with a birefringence one order of magnitude higher than any other fiber structure have been designed and successfully fabricated by introducing a deliberate asymmetry in to the air core [5, 6, 7]. An alternative, opposite approach is to reduce the birefringence by producing fibers with as regular a structure as is possible, in order to exploit the degeneracy between the two linearly polarized FMs of an idealized symmetric PBG structure [8]. It has been demonstrated that (unintentional) deformations during the drawing process can lead to significant mode splitting, resulting in beat lengths of the order of a few mm [9]. Subsequent systematic studies have revealed that even in less obviously asymmetric structures significant polarization dependent phenomena can be observed in the wavelength region where an anticrossing ([10]) occurs between an air-guided core mode (CM) and a surface-localized

#8732 - $15.00 USD Received 8 September 2005; revised 25 October 2005; accepted 25 October 2005

mode (SM). Near-field images of the output mode distribution in such circumstances have shown the presence of spectral regions within the photonic bandgap where one of the two polarizations of the FM appears to interact more strongly with a surface mode than the other [11]. Moreover, an extensive study of the polarization properties of PBGFs has demonstrated a correlation between a peak in the PDL measurement and the presence of a surface mode inside the bandgap at a wavelength where only one of the two polarizations of the fundamental mode appears to be properly guided [12].

In order to generate a deeper understanding of these experimentally observed phenomena we have carried out a number of simulations of a PBGF on which an incremental asymmetric structural perturbation is applied. These examples allow us to deduce more generally how the fiber's polarization properties depend on structural deformations. We demonstrate that many of the recently measured wavelength-dependent polarization properties of PBGFs, such as beat-length and PDL, can be explained by an asymmetry associated with the fiber core combined with the presence of surface modes inside the bandgap.

2. Structure definition and simulation parameters

The structure considered in this study is an ideal representation of a real, state-of-the-art hollow core PBGF in which the central 7 capillaries have been omitted in order to create the mode-guiding defect (Fig. 1).

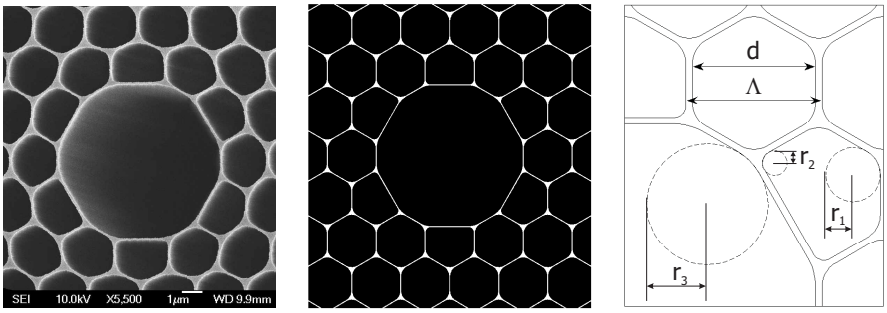

(a) (b) (c)

Fig. 1. (a) SEM image of a typical PBGF produced at our facilities; (b) idealized cross section of the PBGF under investigation; (c) main parameters for the definition of the simulated structure.

The periodic holes, arranged on a triangular lattice to form the photonic crystal, are modeled as hexagons with rounded corners using the representation proposed in Ref. [13], and the parameters best matching a specific PBGF much studied in the literature [14, 15]. The hole-to-hole distance is $\Lambda = 4.7\ \mu$m, the hole diameter d is 0.98Λ, and the corners are rounded with circles of radii $r_1 = 0.22\Lambda$ and $r_2 = 0.1\Lambda$ [Fig. 1(c)]. In order to accurately represent the transverse shape of fibers in which the core is obtained by simply omitting the 7 central capillaries [Fig. 1(a)] we employ a definition for the innermost boundary surrounding the central air region that is slightly different to that used in Ref. [14]. In our representation the core boundary is modeled as a dodecahedron which generates a silica "ring" of the same thickness as the inter-hole struts around the core, and whose corners have been rounded using a circle with radius $r_3 = 0.47\Lambda$. Dielectrics are modeled using the Sellmeier equation for the silica structure and considering n = 1 for air. All the simulations are conducted using a full-vector finite element model, which has already proven to be a fast and accurate tool for simulating index-guiding microstructured fibers [16]. The bandgap of this idealized structure matches quite closely that of the fiber reported in Ref. [14], extending from nearly 1.35 to 1.8 μm, although the position of the surface modes within the bandgap is somewhat different due to the slightly modified core design.

#8732 - $15.00 USD Received 8 September 2005; revised 25 October 2005; accepted 25 October 2005

3. Results

3.1. Perfect Structure

The effective index plot in Fig. 2 presents the dispersion of the modes, either localized in air or on the surface terminating the photonic crystal, whose frequency lies within the photonic bandgap for the case of a perfectly symmetric, unperturbed structure. One very evident avoided crossing takes place near the middle of the bandgap between pairs of linearly polarized modes (solid blue lines). This involves the degenerate pair of HE_{11}-like, air-guided, fundamental modes passing through points (a), (b), (g) and (h), and the two degenerate, linearly polarized SMs passing through (e) and (d).

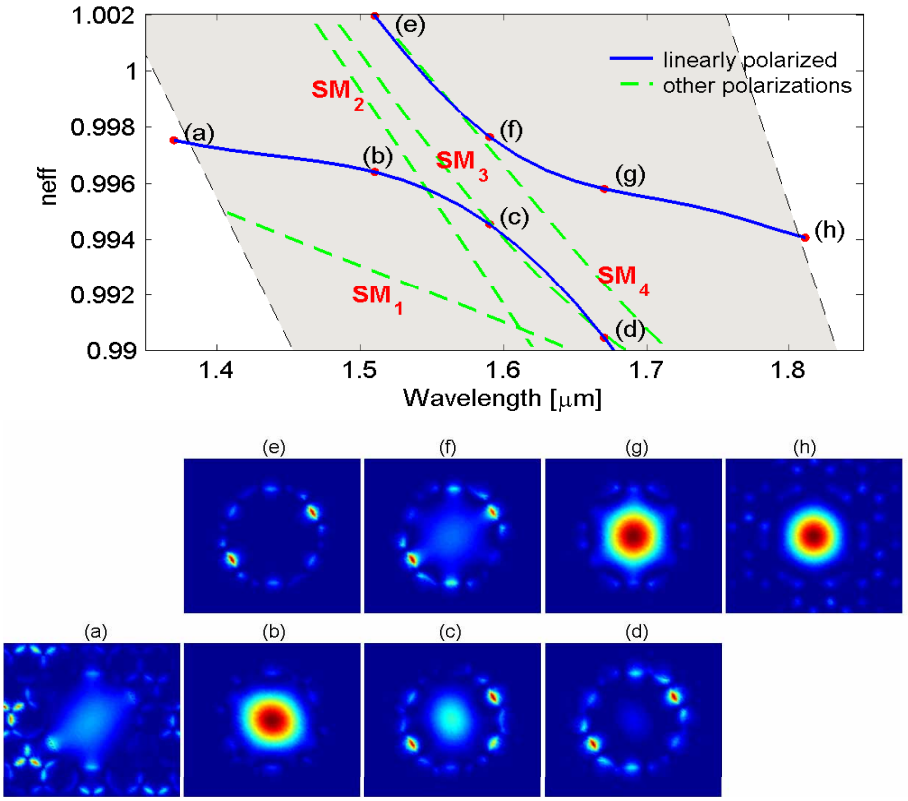

Fig. 2. (Top) Effective index plot for the perfectly symmetric structure. The shaded area represents the bandgap as calculated for an infinite periodic cladding; (Bottom) Poynting vector of a linearly polarized mode: (a) and (h) are at the bandgap edges, while (b)→(d) and (e)→(g) show the mode evolution in the two branches of the anticrossing.

The large separation in effective index between the interacting modes around the avoided crossing at $\lambda = 1.6\ \mu$m is an indication of a large interaction between the modes involved [10]. Besides the SM shown at points (d) and (e), other SMs (represented by dashed green lines) are supported by this structure, but since they belong to different symmetry classes they do not significantly interact with the linearly polarized fundamental modes. The 8 subplots at the bottom of Fig. 2 show the evolution of the mode's Poynting vector from the bandgap edge to the central avoided crossing region and vice versa.

#8732 - $15.00 USD Received 8 September 2005; revised 25 October 2005; accepted 25 October 2005

3.2. *Perturbed structure*

In order to understand how the PBGF polarization properties depend upon structural imperfections, we consider the consequence of two different deformations of the fiber cross-section, as shown in Fig. 3. The first (deformation A) is obtained by scaling the whole structure in the x direction only, according to

$$(x,\, y) \rightarrow \left(x \cdot [1+f]\,, y\right) \tag{1}$$

where f is the percentage scaling factor. Deformation A thus generates an oval fiber with an oval core and a correspondingly modified periodic cladding.

For deformation B we distort only the dodecahedron defining the inner boundaries of the core by compressing it in the x direction and leaving the periodic cladding unaltered. The deformation is defined by

$$(x,\, y) \rightarrow \left(x \cdot \left[1 - f \cdot \frac{\Lambda - d}{Lc}\right]\,, y\right) \tag{2}$$

where Lc is the core radius of the unperturbed structure. In this way f represents the (percentage) thickness variation of the vertical struts around the air core. The thickness of the diagonal struts linearly decreases to that of the (unaltered) horizontal struts.

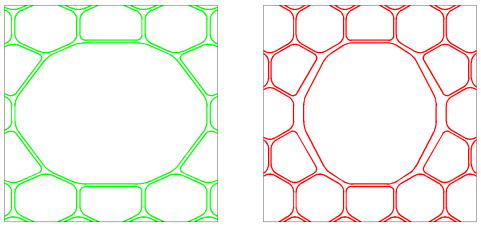

(A) (B)

Fig. 3. Deformation types considered: (A) overall deformation with f = 30%; (B) core deformation with an exaggerated f = 300% for illustration purposes.

Applying either deformation distorts the silica ring around the core such that the thickness of the vertical struts is scaled by a factor (1 + f) whilst the thickness of the horizontal upper and lower struts remains unchanged. Since this ring is where surface modes are located it comes as no surprise that for both types of deformation we obtained qualitatively similar anticrossing behavior for the same value of f. This can be seen by comparing the effects of deformation A in Fig. 4(a) and (b) with those of deformation B in Fig. 5(a) and (b). Deformation A however also distorts the periodic cell, resulting in a narrowing and shifting of the bandgap to longer wavelengths. Moreover it also has the effect of scaling the ratio between the geometric core axes by a factor (1 + f) which is more than 2 orders of magnitude larger than that due to deformation B. As can be seen in Fig. 4 this has the effect of introducing a large amount of "ordinary" birefringence between the core modes as previously reported [9]. In order to avoid any effects arising from the deformation of the bandgap itself, and to better identify those polarization effects arising from coupling to SMs, we focus the rest of the paper on the influence of deformation B. We do however believe that the overall conclusions that we have obtained can be generalized to any similar asymmetric deformation of the inner silica ring, including deformation A.

Figure 5 shows the effect of applying deformation B with f = 5%, 10%, 20% and 30% to the fiber in Fig. 1. The unperturbed fiber had a core silica ring thickness of (Λ - d) = 94 nm. Note that the increase in thickness introduced (4.7, 9.4, 18.8 and 28.2 nm respectively) is around 2

#8732 - $15.00 USD Received 8 September 2005; revised 25 October 2005; accepted 25 October 2005

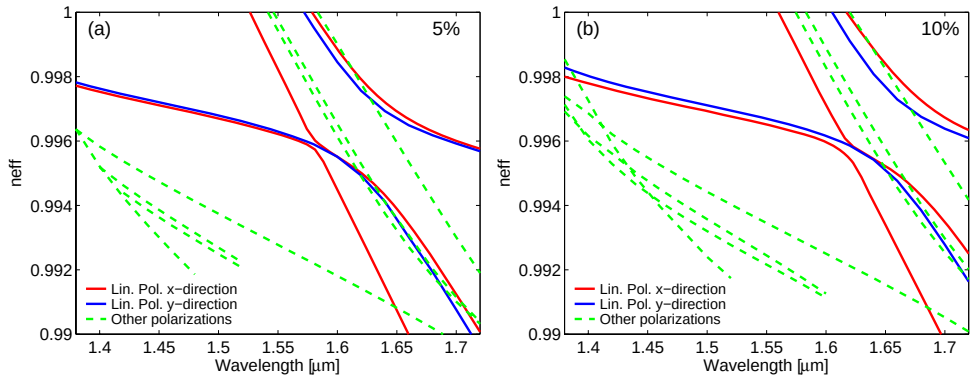

Fig. 4. Effect of deformation A with f = 5% and f = 10%. Linearly polarized modes are represented with solid lines, while dashed lines are used for any other polarization type.

orders of magnitude smaller than the wavelength of light and 3 orders of magnitude smaller than the fiber's core. In ordinary waveguiding structures this would be expected to represent an almost negligible variation. For example, our calculations show that for an index guiding holey fiber with the same pitch (Λ = 4.7 μm) and d/Λ = 0.4, adding 9.4 or 18.8 nm to the pitch length in just the x-direction causes the birefringence to increase from our numerical resolution limit of $\Delta n \leq 1.5{\cdot}10^{-7}$ for the perfect structure to just $3.5{\cdot}10^{-7}$ and $8.7{\cdot}10^{-7}$ respectively.

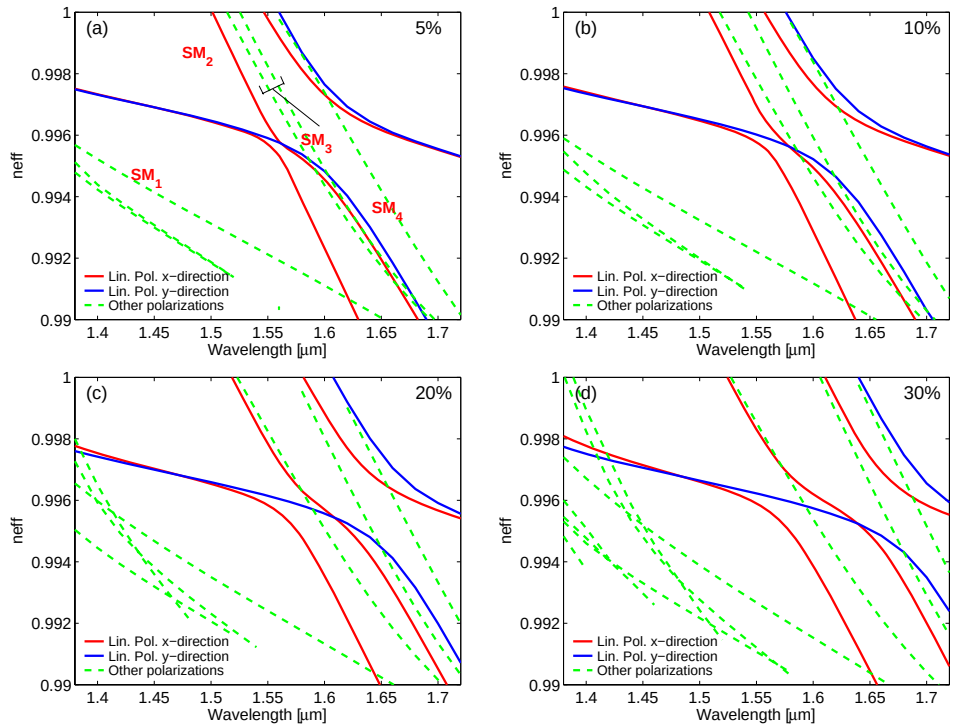

Fig. 5. Effect of deformation B, producing an increase of 5%, 10%, 20% and 30% on the thickness of vertical struts around the core.

#8732 - $15.00 USD Received 8 September 2005; revised 25 October 2005; accepted 25 October 2005

In hollow core PBGFs the termination of the cladding periodicity around the central defect localizes a number of surface modes at the photonic crystal termination. These modes, localized in regions of the thin silica ring around the core and exponentially decaying on either side of it [Fig. 2(e)], are extremely sensitive to the precise level of structural deformation applied, as can be appreciated by studying Fig. 5(a)-(d). Moreover, through an avoided crossing mechanism [10], the core mode can also become extremely sensitive to small scale structure variations.

From a group representation theory point of view, as a consequence of the deformation, the structure shifts from a symmetry class C_{6v} to C_{2v} (a general random perturbation would destroy any symmetry, but this doesn't change the final result of the present study) [17]. As a result, the 4 non-degenerate symmetry classes which exhibit the full waveguide symmetry in C_{6v} are no longer supported, and the 4 remaining classes become non-degenerate. Both these effects can be observed by comparing Fig. 2 and Fig. 5(a). In the perfect structure the SM denoted as SM_2 belongs to a class exhibiting the full 6-fold fiber symmetry (using the same nomenclature as for the core modes it would be labeled as HE_{31y}), while SM_3 represents a pair of degenerate surface modes (HE_{21}). After the deformation is introduced the SM_3 modes are split, while SM_2 is transformed into a linearly polarized mode, interacting with only one of the fundamental modes. Also the linearly polarized SMs which interacted with the FMs in the perfect structure split, causing the avoided crossings for the 2 polarizations to take place at different wavelengths.

Increasing the amount of deformation has a different effect on the 2 polarizations, as can be observed in Fig. 6.

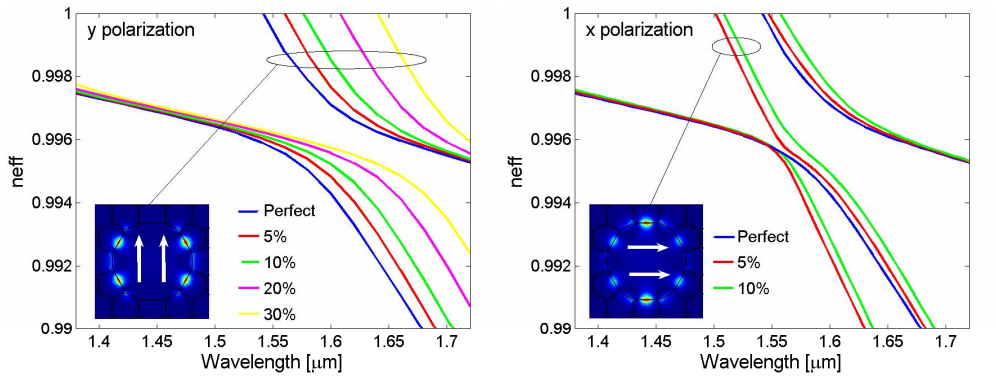

Fig. 6. Effect of core deformation on the mode having the transverse electric field polarized along the y (left) and x axis (right). The insets show the surface mode involved in the anticrossing.

The SM whose electric field is linearly polarized along the y-axis concentrates its power on the lateral silica struts, whose thickness is progressively increased (Figure 6, left). As a result the effective index of the mode increases with the thickness, shifting the avoided crossing to longer wavelengths. A different behavior can be noticed for the x-polarized modes (Figure 6, right). Here the structural perturbation introduces a second linearly polarized surface mode, SM_2, initially very weakly interacting with the FM. As the deformation is increased though, the degree of polarization (DOP) of SM_2 also progressively increases, resulting in a stronger interaction with the fundamental mode. A difference in the wavelength dependent loss for each polarization will clearly be associated with this behavior.

According to the results of the coupled mode theory-based model proposed to evaluate the overall losses due to a SM-CM interaction, each avoided crossing generates a peak with

#8732 - $15.00 USD Received 8 September 2005; revised 25 October 2005; accepted 25 October 2005

Lorentzian shape in the loss spectrum. The peak width is inversely proportional to the difference in propagation constant between the modes involved in the avoided crossing $\Delta\beta_{ij}$, and each Lorentzian loss peak is given by [19]:

$$Loss(dB/m) \sim \gamma_i \cdot \frac{|\kappa_{ij}|^2}{(\Delta\beta_{ij})^2} \tag{3}$$

where γ_i is the loss coefficient due to coupling between SM_i, and a continuum of leaky cladding modes and κ_{ij} describes the coupling between SM_i and FM_j. In order to acquire a qualitative understanding of the (unweighted) contribution to the overall loss due to the SM-CM interaction we plot in Fig. 7 the factor $|\kappa_{ij}|^2/(\Delta\beta_{ij})^2$ for the two polarizations and different levels of distortion.

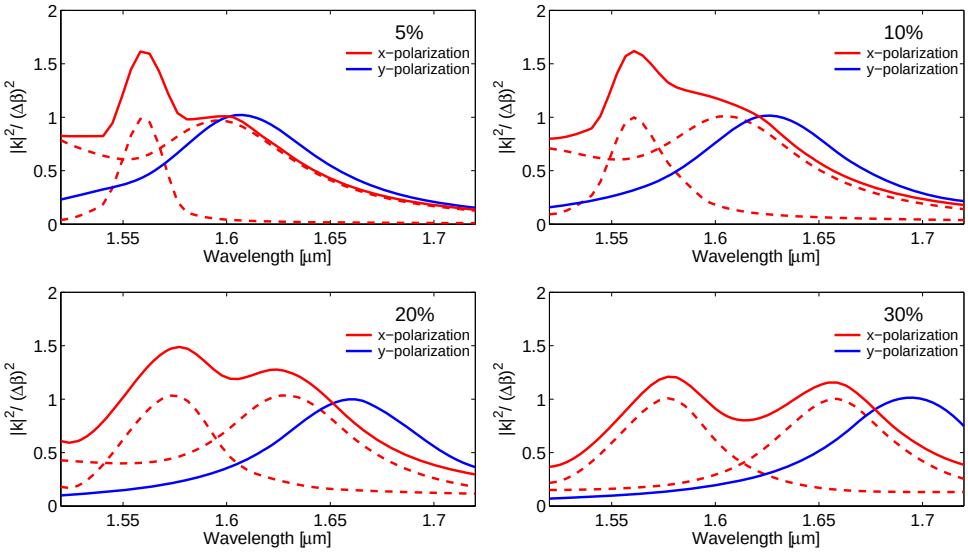

Fig. 7. The set of Lorentzian peaks proportional to the loss induced by avoided crossings in the two polarizations for different levels of structural deformation. The dashed lines represent single peaks while the continuous lines show the total contribution for each polarization.

The derivation of the exact γ_i for each SM goes beyond the scope of this paper but as a first approximation γ_i can be considered constant for all surface modes as previously demonstrated in Ref. [20] where a good fit to measured loss data was achieved using this assumption. Therefore we believe that from Fig. 7 it can be qualitatively appreciated how even a small-scale perturbation from the perfect structure can introduce significantly different losses for the two polarization states. This can explain the large value of PDL measured in Ref. [12] for wavelengths well inside the bandgap in the vicinity of a surface mode. The fiber used in these experiments exhibits a clear core asymmetry and, just as for the fiber studied in Fig. 5(d) at wavelengths around 1.6 μm, this could well have resulted in an anticrossing between the FM and a SM in just one of the two polarization states.

To conclude the analysis we calculate the beatlength for a fiber with a distorted core of f = 10% (Fig. 8). Far from the anticrossing region, at both shorter and longer wavelengths, only one pair of orthogonal modes is supported in the air core. The beatlength is therefore unequivocally defined, and it presents a strong wavelength dependent behavior, arising principally from the

#8732 - $15.00 USD Received 8 September 2005; revised 25 October 2005; accepted 25 October 2005

different wavelength locations of the anticrossing for the two polarizations. This is in accordance with the experimental observation in Ref. [12], where a mean beatlength of 1.1 cm was also measured at a wavelength 70 nm away from an anticrossing.

In the region where avoided crossings for the orthogonal polarizations take place at different wavelengths, i.e. between the vertical dashed lines in Fig. 8, the definition of beatlength becomes ambiguous. This is due to the presence of two or more modes per polarization with different propagation constants but similar transverse profiles and mode overlap with the air core (such as modes (c) and (f) in Fig. 2). A superposition of those modes is likely to be excited in practical experiments, and therefore, between approximately 1.55 and 1.67 μm, more than one beatlength can be theoretically defined [Fig. 8 (bottom)], and in principle measured. Generally though, when launching light into these fibers, the coupling is optimized so that the air guided modes are predominantly excited. Under these circumstances we would expect principally the beatlengths corresponding to wavelengths where both interacting modes have a high percentage of power in air to be measurable, such as, in Fig. 8 (bottom), the region around 1.57 μm for modes x_2 and y_1 (green curve) or around 1.62 μm for x_3 and y_1 (red curve). In practice however, randomly distributed perturbations of the core boundary or 'point-defects' along the fiber length may cause random shifts of the position of the SM within the bandgap, making it difficult to make birefringence or beatlength measurements in the vicinity of the anticrossing, as possibly witnessed during the PBGF birefringence measurements reported by Chen et al. [Ref. [6], Fig. 5(a)].

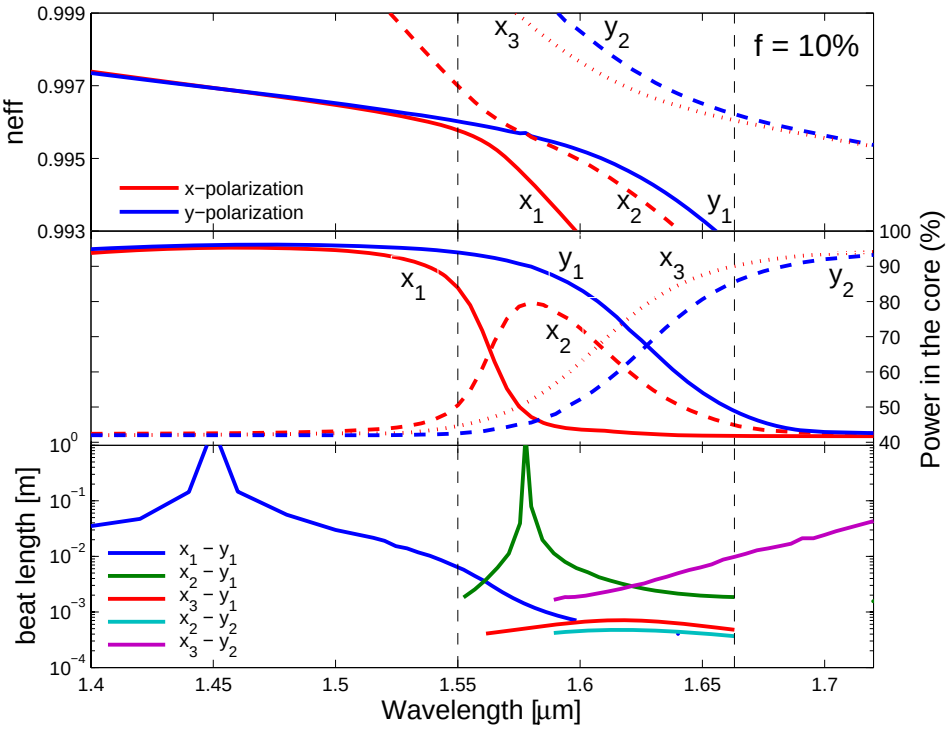

Fig. 8. Effective index (Top) and percentage of the mode in the core (Middle) for the 5 modes involved in three different anticrossings for a fiber with a 10% distortion; (Bottom) Calculated beatlength for various interactions between an x and y polarized mode.

#8732 - $15.00 USD Received 8 September 2005; revised 25 October 2005; accepted 25 October 2005

Theoretically calculated values of beatlength as short as a few mm or less for the PBGF in this study may be surprising at first, considering that the structural perturbation introduced is nearly 1000 times smaller than the period of an otherwise perfectly symmetric structure. This is another consequence of the extreme sensitivity of this type of fiber to structural imperfections at the interface between defect and photonic crystal.

4. Discussion and conclusions

We have shown, through full vector simulations of a hollow core PBGF, that large and noticeable effects on the fiber's polarization properties can be produced not only by macroscopic structural deformations, but also by small asymmetries in the shape of the silica ring surrounding the core, where surface modes are located.

Previous experimental observations of anomalous polarization behavior in PBGFs, including the measurement of a strongly wavelength dependent beatlength and polarization dependent loss [12] can be explained by the results presented in this study. Moreover, the observed changes in mode profile as a function of polarization and wavelength reported in Ref. [11] can be explained by assuming that avoided crossings for the two polarizations occur at slightly different wavelengths due to an (even small) asymmetric structural deformation of the core. Under such circumstances, we have shown through a specific example that multiple beatlengths should be theoretically measurable, resulting from the fact that in experiments a superposition of modes with slightly different effective indices would be excited at a given wavelength. We speculate though that due to the presence of 'point defects' or small non-uniformities along the fiber length, a clear measurement of those multiple beatlengths may be problematic [6].

Information about the fiber's birefringence around an anticrossing region may not be important for many applications of PBGFs, particularly if the fiber is operated at wavelengths away from any anticrossing region or it is designed not to have surface modes. However in the future, assuming an improved understanding of anti-crossing behavior and likely advances in PBGF fabrication, it may be possible to exploit the various phenomena we have described in order to tailor the birefringence and PDL of PBGFs to suit specific applications.

This study highlights the fact that, due to the presence of surface modes, the polarization properties of hollow core PBGF can be strongly affected by structural features and distortions with length scales around 2-3 orders of magnitude smaller than the cladding periodicity. It is to be appreciated that the dispersive properties of such fibers can show a similar level of structural sensitivity for the same reasons. The ability to control the shape of core structures over 3 orders of magnitude could thus represent a key challenge in the future realization of optimized hollow-core PBGFs.

Acknowledgments

The authors would like to thank Dr. M. N. Petrovich, Dr. V. Finazzi and R. Amezcua-Correa for providing some data for the study and for useful discussions.

#8732 - $15.00 USD Received 8 September 2005; revised 25 October 2005; accepted 25 October 2005